Chemical Science

EDGE ARTICLE

Photochemical charge accumulation in a heteroleptic copper(I)-anthraquinone molecular dyad *via* proton-coupled electron transfer†

Zhu-Lin Xie, [ID] [a] Nikita Gupta, [ID] [ab] Jens Niklas, [ID] [a] Oleg G. Poluektov, [ID] [a] Vincent M. Lynch,[c] Ksenija D. Glusac [ID] [ab] and Karen L. Mulfort [ID] *[a]

Developing efficient photocatalysts that perform multi electron redox reactions is critical to achieving solar energy conversion. One can reach this goal by developing systems which mimic natural photosynthesis and exploit strategies such as proton-coupled electron transfer (PCET) to achieve photochemical charge accumulation. We report herein a heteroleptic Cu(I)bis(phenanthroline) complex, **Cu-AnQ**, featuring a fused phenazine-anthraquinone moiety that photochemically accumulates two electrons in the anthraquinone unit *via* PCET. Full spectroscopic and electrochemical analyses allowed us to identify the reduced species and revealed that up to three electrons can be accumulated in the phenazine-anthraquinone ring system under electrochemical conditions. Continuous photolysis of **Cu-AnQ** in the presence of sacrificial electron donor produced doubly reduced monoprotonated photoproduct confirmed unambiguously by X-ray crystallography. Formation of this photoproduct indicates that a PCET process occurred during illumination and two electrons were accumulated in the system. The role of the heteroleptic Cu(I)bis(phenanthroline) moiety participating in the photochemical charge accumulation as a light absorber was evidenced by comparing the photolysis of **Cu-AnQ** and the free AnQ ligand with less reductive triethylamine as a sacrificial electron donor, in which photogenerated doubly reduced species was observed with **Cu-AnQ**, but not with the free ligand. The thermodynamic properties of **Cu-AnQ** were examined by DFT which mapped the probable reaction pathway for photochemical charge accumulation and the capacity for solar energy stored in the process. This study presents a unique system built on earth-abundant transition metal complex to store electrons, and tune the storage of solar energy by the degree of protonation of the electron acceptor.

Introduction

Photocatalysis targeted at CO_2 reduction, hydrogen evolution and water oxidation for solar energy conversion has drawn considerable attention due to the finite amount of fossil fuels and the aggravated outcome of their combustion.[1–5] Since these reactions involve transferring multiple electrons/holes as energetic products are generated, efficient photocatalysis can be difficult to achieve if traditional catalysts that operate in single-electron transfer mechanism are utilized.[6–8] This issue can be addressed by developing catalytic systems that operate *via* photochemically accumulated charge transfer steps coupled with proton transfers, the strategy employed by natural

photosynthesis. In nature, the oxygen evolving center (OEC) in photosystem II (PS II) undergoes four proton-coupled electron transfer (PCET) processes induced by photoexcitation, which accumulates oxidative equivalents for molecular oxygen generation and avoids the formation of high energy intermediates.[9–12] The electrons are transferred through a cascade of cofactors, which include quinones, the important electron carriers that accept two pairs of electrons and protons after electron transfer processes.[13–15] At the end of the electron transfer chain, $NADP^+$ is reduced with two electrons and one proton, and the resulting NAPH molecules are eventually used in the Calvin cycle for CO_2 assimilation.[16,17] The combination of charge accumulation and PCET renders the natural photosynthetic system efficient and robust, which converts solar energy into chemical fuels.

Biomimetic donor–acceptor assemblies have provided a fundamental understanding of how to integrate and control photochemical charge accumulation and PCET in photocatalytic systems.[6,7] The first molecular system that implements photochemical charge accumulation and PCET was reported by Konduri *et al.*[18,19] In these studies, two dinuclear Ru(II) complexes with extended π-conjugated bridging ligands based

[a]*Division of Chemical Sciences and Engineering, Argonne National Laboratory, USA. E-mail: mulfort@anl.gov*

[b]*Department of Chemistry, University of Illinois at Chicago, USA*

[c]*Department of Chemistry, University of Texas at Austin, USA*

† Electronic supplementary information (ESI) available. CCDC 2278029 2278030. For ESI and crystallographic data in CIF or other electronic format see DOI: https://doi.org/10.1039/d3sc03428c

on phenazine and/or quinone demonstrated reversible charge accumulation of two and four electrons, respectively, upon photoexcitation in the presence of a sacrificial electron donor. Protonation of the nitrogen or oxygen atoms at the central ligand was shown to couple with the formation of the reduced product by the mechanism of two sequential one-electron processes under basic conditions, or a bielectronic process under neutral or slightly acidic conditions.[20] Later, the Wenger group developed a covalently-linked unconjugated pentad complex (TAA-Ru-AQ-Ru-TAA) composed of triarylamine (TAA), Ru tris-bipyridine and the anthraquinone (AQ) and demonstrated that the charge-separated state with two electrons stored at the anthraquinone moiety was accessed upon photo-illumination.[21,22] Importantly, a considerably longer lived charge-separated state was observed under acidic conditions[21] than in neat solvent.[22] These studies underscore a key benefit of PCET, namely, stabilization of a highly reduced species which leads to improvement in the lifetime of the charge accumulated state. However, this increased stability of the protonated, charge-separated state is often achieved with a coincident decrease in energy, essentially reducing the possible amount of solar energy that could be used for fuels catalysis. A potential solution to this issue is to store photogenerated electrons at more reducing potentials by judicial design of the structure of the donor–acceptor assembly. This has been manifested, for example, in the $[(phen)_2Ru(tatpp)Ru(phen)_2][PF_6]_4$ system[23] by changing the bridging linear tetraazapentacene ligand into one with a 120° bend which resulted in a ~500 mV negative shift of the reduction potential of the ligand, or in Ru-dipyridonphenazine-pyridoquinolinone system[24,25] by modifying the pyridoquinolinone moiety to a pyridoquinolinone-oxime derivative, inducing a negative shift of the first and second reduction potential by −0.24 V and −0.14 V, respectively. These reports exemplify that effective structural modification of the acceptor can alter the molecular electrochemical response so that optimal photochemical charge accumulation systems with high energy conversion efficiency can be achieved.

The examples described above have provided important insight into the molecular design components needed to support PCET-enabled charge accumulation, although these and several other examples are all built upon the Ru(II)tris(bipyridine) photosensitizer module.[26–29] The photoactive Ru(II) center has shown outstanding photophysical and photochemical properties, but the use of precious metals prevents the application of such molecular systems to sustainable large-scale catalysis,[30] yet there are few reports describing photochemical charge accumulation achieved without precious metals.[31,32] Among the first-row photoactive transition metal complexes, Cu(I)diimine complexes are of special interest and have been regarded as a potential substitute for the quintessential Ru(II)poly(pyridyl) photosensitizers.[33–35] The d^{10} Cu(I) center allows the Cu(I)diimine complexes to access the metal-to-ligand charge transfer (MLCT) state by absorbing visible light ranging from 400 to 550 nm.[35] The excited state lifetimes of Cu(I)diimine complexes were historically shorter than Ru(II)poly(pyridyl) complexes,[33,36] but a large and growing literature has explored ligand designs that can extend their excited state lifetimes well into the microsecond regime.[37–41]

Chart 1 Photoactive heteroleptic Cu(I) complexes studied in this paper, **Cu⁺-AnQ** and **Cu⁺-DPPZ**. Superscripts indicate charges carried by Cu. The notation of the mesPhen ligand is omitted from the naming system as it is not the focus of this study.

Furthermore, the ease of oxidation of the Cu(I) center results in these complexes acting as strong electron donors during photochemical processes.[42–44] These exceptional electro- and photochemical features of the Cu(I)diimine complexes have gained interest for their applications in dye-sensitized solar cells,[30] photocatalysis,[45] and light emitting diodes,[46] for example.

In this report, we describe the first molecular donor–acceptor assembly, **Cu⁺-AnQ**, built upon a Cu(I)diimine chromophore fused with phenazine-anthraquinone (AnQ) moiety for photochemical charge accumulation (Chart 1). We demonstrate that, upon visible light illumination, the extended π-conjugation of the AnQ ligand is capable of storing two electrons at the anthraquinone moiety in the presence of a sacrificial electron donor via a PCET process, which generates the doubly reduced, monoprotonated product **Cu⁺-AnQH⁻** that is stable for at least 24 hours. DFT calculations show that the basicity of **Cu⁺-AnQH⁻** is significantly lower than the basicity of the doubly reduced, unprotonated species **Cu⁺-AnQ²⁻** because of the unique curvature designed into the ligand. As a result, monoprotonation of **Cu-AnQ** not only stabilizes the photogenerated two-electron reduced state, but also avoids substantial energy loss associated with protonation. This study demonstrates a distinct strategy for improving the yield of solar energy conversion in molecular systems by controlling the protonation state of photoproducts and provides important foundational knowledge for integrating photochemical charge accumulation in photocatalytic systems.

Results

Molecule design, syntheses and structural characterization

To engineer a charge accumulation site with Cu complexes, we designed the dyad **Cu⁺-AnQ** by utilizing the Cu HETPHEN

strategy, developed by Schmittel *et al.*[47–49] This method is effective for the synthesis of heteroleptic Cu(ɪ)bis(phenanthroline) complexes by using 2,9-dimesityl-1,10-phenanthroline (mesPhen) as a blocking ligand that prevents bis(mesPhen) coordination and allows the ligation of a second, different ligand to the Cu(ɪ) center. Here the second phenanthroline ligand was derivatized to fuse an anthraquinone moiety, forming a π-conjugated dipyridophenazine-anthraquinone ligand (AnQ). The decreasing energy level follows the order of Cu(ɪ) center, phenazine, anthraquinone, and is designed to realize a directional energy cascade from Cu(ɪ) to anthraquinone. The ability of anthraquinone to accept multiple electrons and protons makes **Cu⁺-AnQ** a good candidate for studying charge accumulation and PCET, as demonstrated in similar molecular assemblies based on Ru(ɪɪ) chromophores and anthraquinone, developed by Wenger and coworkers,[21,22,50,51] but importantly here we investigating a model system using only earth-abundant elements. We have also synthesized **Cu⁺-DPPZ** and 2,17-dimethylnaphtho[2,3-*h*]dipyrido[3,2-*a*:2′,3′-*c*]phenazine-8,13-dione (**MeAnQ**) as control molecules to compare with the spectroscopic investigation and photochemical inquiry of **Cu⁺-AnQ**. **MeAnQ** is analogous to the free ligand, **AnQ**, but the methyl groups increase the solubility in acetonitrile from the uncoordinated ligand **AnQ**, whose strong π–π stacking interaction results in very low solubility and prevented us from obtaining the solution phase properties of the ligand.

The synthesis of the **Cu⁺-AnQ** dyad is summarized in Scheme 1 and full details are presented in the ESI.† Briefly, a stoichiometric amount of [Cu(MeCN)₄](PF₆) and mesPhen ligand were mixed in deaerated dichloromethane, producing a yellow solution of [Cu(mesPhen)(MeCN)₂](PF₆). The intermediate was

then treated with one equivalent of 1,10-phenanthroline-5,6-dione (Phendione) to afford the building block [Cu(mesPhen)(Phendione)](PF₆) in 96% yield. Complex **Cu⁺-AnQ** was formed through a condensation between [Cu(mesPhen)(Phendione)](PF₆) and 1,2-diaminoanthraquinone under refluxing conditions in ethanol and a catalytic amount of acetic acid for seven days. Complex **Cu⁺-DPPZ** was synthesized according to the Cu HETPHEN method and following literature precedent[52] for the DPPZ ligand. The ligand **MeAnQ** was synthesized according to the reported procedure.[53]

Proton NMR spectroscopy was employed to identify the target complexes. The NMR shows that the extension of π-conjugation with an anthraquinone moiety does not impact the local electronic environment of the mesPhen protons, as shown by the fact that the proton signals derived from the mesPhen of **Cu⁺-DPPZ** exhibit comparable values with those of **Cu⁺-AnQ** (Fig. S5 and S7†). However, the coordination of AnQ to [Cu(mesPhen)]¹⁺ breaks the C_2 symmetry of the complex, resulting in a splitting of the proton signals from mesPhen. Also, we observe significant downfield shifts for the protons in the immediate phenanthroline moiety of the AnQ ligand as compared to that for DPPZ (protons H_3, $H_{3'}$, H_4, H_5 in Fig. S5 and S7†). The change of chemical shift is related to the anthraquinone moiety which acts as an electron withdrawing group that pulls electron density away from the DPPZ moiety.

The crystal structure of **Cu⁺-AnQ** was obtained *via* vapor diffusion of diethyl ether to an acetonitrile solution of **Cu⁺-AnQ**. Fig. 1A shows that the Cu(ɪ) center is coordinated with four N atoms from two ligands in a pseudo-tetrahedral geometry with an s_4 value of 0.67 (1 for perfect tetrahedral and 0 for perfect square planar[54]). The C=O bond distances on the AnQ ligand

Scheme 1 Synthesis of **Cu⁺-AnQ**, **Cu⁺-DPPZ** and **MeAnQ**.

are 1.223(2) and 1.217(2) Å, confirming the double bond nature of the carbonyl group and are comparable to the literature values for quinone molecules.[21] The bond distances of Cu–N range from 1.99 to 2.09 Å, with the two Cu–N bonds to mesPhen being both the shortest and the longest in the structure (1.9967(15) Å, 2.0910(15) Å). This derives from the significant structural distortion of mesPhen coordination, where the mesPhen ligand binds with the Cu(I) center in the "pacman" orientation.[55] This preferential orientation in the solid state results in one mesityl aryl ring that stacks with the AnQ ligand plane through π–π interactions and the other aryl ring dangles away, avoiding being parallel with the AnQ ligand. This distortion paves the way for **Cu⁺-AnQ** to form dimer structures in crystal lattice, shown in Fig. 1B. The dimers in the solid phase arise through the π–π interactions between the two AnQ ligand planes with a distance of 3.398 Å. Together with the interactions between the mesityl groups and the AnQ ligands, individual complexes are piled forming 1D columns in the crystal lattice (Fig. S14 and S15†).

The dimer formation observed in the solid state structure persists to some extent in the solution phase, as confirmed by a concentration dependence of the ¹H NMR peak shifts for both **Cu⁺-AnQ** and **Cu⁺-DPPZ**. The protons from AnQ and DPPZ show an upfield shift as their concentration in CD₃CN increases (Fig. S11 and S12†), which suggests dimerization of individual molecules in the solution state as depicted in Fig. 1C. Such dimerization in the solution state has been observed in Ru(II) and Os(II) complexes coordinated to planar extended π-conjugated ligands, such as TPPHZ[56,57] and eilatin.[58,59] These complexes tend to stack in head-to-tail fashion *via*

intermolecular π–π interactions by the π-conjugated ligands. The dimer model[60,61] was used to fit the shift of the proton signals yielding an association constant $K_D = 61.3$ for **Cu⁺-AnQ** and 3.7 for **Cu⁺-DPPZ** (for details see ESI†). An important implication of the different ability of the two complexes to form dimers is that for a given concentration, a larger fraction of **Cu⁺-AnQ** occurs as a dimer than does **Cu⁺-DPPZ**. As shown in Fig. 1D, it is evident that at a concentration of 0.2 mM there is 99% of **Cu⁺-DPPZ** exists as monomer and 97% of **Cu⁺-AnQ** is in the monomer form. Therefore, we kept both complexes at 0.2 mM for subsequent electro/photochemical studies to avoid the impact of dimerization on these properties.

Steady state optical and electrochemical characterization

The steady state UV-vis spectra of **Cu⁺-AnQ** and **Cu⁺-DPPZ** in acetonitrile solution exhibit metal-to-ligand charge transfer (MLCT) bands at around 460 nm (Fig. 2A and Table 1). However, **Cu⁺-AnQ** displays stronger MLCT absorption, which is about 45% more intense than that of **Cu⁺-DPPZ**. In the UV region, we observe moderately structured bands at 385 and 401 nm for **Cu⁺-AnQ** and 356 and 374 nm for **Cu⁺-DPPZ**, which are assigned to ligand centered (LC) transitions, with **Cu⁺-AnQ** presenting higher absorbance in these transitions. The red-shift of the LC transition from **Cu⁺-AnQ** clearly indicates that the AnQ ligand has lower energy level than DPPZ due to the extended π-conjugation that includes the anthraquinone moiety. Further, the LC band of **Cu⁺-AnQ** aligns with the absorption of the uncoordinated ligand **ᴹᵉAnQ**, suggesting that the Cu ligation does not impact the local electronic property of the ligand, the evidence of electronic decoupling between the Cu center and ligand.

Fig. 1 (A) ORTEP diagram of **Cu⁺-AnQ** (50% thermal ellipsoids; all hydrogen atoms and the counterion PF₆⁻ are omitted for clarity). (B) Dimer structure of **Cu⁺-AnQ** in crystal lattice. (C) Schematic presentation of dimerization of **Cu⁺-AnQ** in acetonitrile. (D) Calculated molar fractions of dimer and monomer **Cu⁺-AnQ** and **Cu⁺-DPPZ** in acetonitrile affected by the total concentration of the complex. The calculation was based on the association constant K_D.
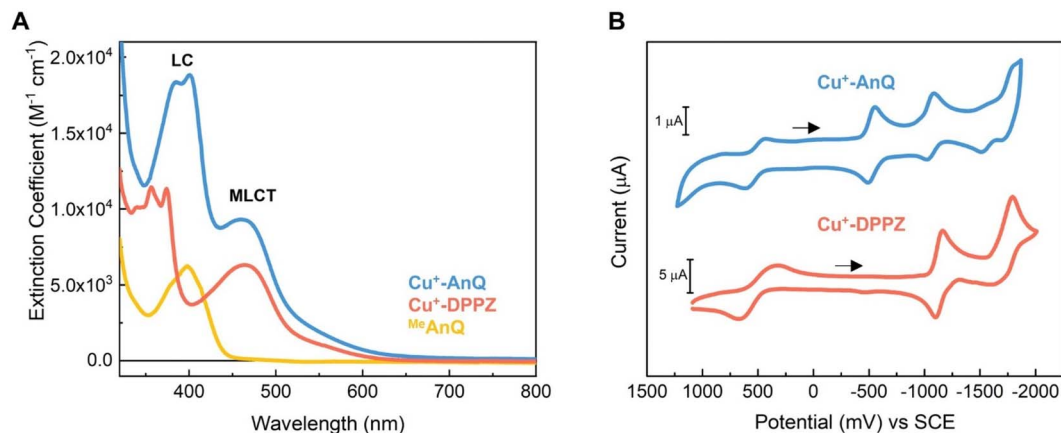
Fig. 2 (A) Experimental UV-vis spectra of **Cu⁺-AnQ**, **Cu⁺-DPPZ** and **ᴹᵉAnQ** in acetonitrile (concentrations of the measurements were kept below 0.2 mM); (B) cyclic voltammogram of **Cu⁺-AnQ** and **Cu⁺-DPPZ** in acetonitrile (0.2 mM for **Cu⁺-AnQ**, 1 mM for **Cu⁺-DPPZ**, 0.1 M TBAPF₆; working: Pt disc, counter: Pt wire, reference: Ag/Ag⁺ non-aqueous with ferrocene as internal standard; scan rate = 100 mV s⁻¹; arrows indicate the direction of the scan).

Table 1 Summary of optical and electrochemical characterization of **Cu⁺-AnQ** and **Cu⁺-DPPZ**

Complexes	λ_{max}/nm (ε/M⁻¹ cm⁻¹)	E (Cu²⁺/¹⁺) (V vs. SCE)	E (Q⁰/¹⁻)[a] (V vs. SCE)	E (Q¹⁻/²⁻)[a] (V vs. SCE)	E (Phz⁰/¹⁻)[a] (V vs. SCE)	E (BL⁰/¹⁻)[a] (V vs. SCE)
Cu⁺-AnQ	385 (18 361), 401 (18 817), 461 (9304)	+0.52	−0.53	−1.05	−1.55	−1.77
Cu⁺-DPPZ	356 (11 435), 374 (11 330), 464 (6319)	+0.50			−1.13	−1.70

The electrochemical properties of **Cu⁺-AnQ** and **Cu⁺-DPPZ** were characterized by cyclic voltammetry (CV) in acetonitrile containing 0.1 M tetrabutylammonium hexafluorophosphate (TBAPF₆) as the electrolyte (Fig. 2B and Table 1). Both complexes exhibit a quasi-reversible Cu(ɪɪ/ɪ) redox couple at +0.52 V vs. SCE for **Cu⁺-AnQ** and +0.50 V vs. SCE for **Cu⁺-DPPZ**. The quasi-reversibility of the Cu oxidation is a result of the pseudo Jahn–Teller distortion of Cu(ɪɪ) center, which flattens the coordination geometry of Cu from tetrahedral towards square planar.[62–64] In addition, the almost identical oxidation potential found in both complexes indicates that the Cu centers of **Cu⁺-AnQ** and **Cu⁺-DPPZ** have similar electronic structure, which is attributed to the negligible electronic influence from the anthraquinone moiety due to the long distance between the Cu center and anthraquinone moiety. Such weak electronic coupling has been observed in other Ru/Os/Cu bimetallic complexes with two metals bridged by TPPHZ-like ligands;[62,65] this further exemplifies that although the π-electrons in the ring system might act as a "wire" for excited state electron transfer, the ground state electronic environment of the metal center remains relatively localized at the first and second coordination sphere.

Turning to the reduction side, **Cu⁺-AnQ** exhibits four ligand-based reductions. The first two reductions with $E_{1/2}$ = −0.53 V and −1.05 V vs. SCE are assigned to the first and second reductions of the anthraquinone moiety, generating the singly reduced **Cu⁺-AnQ⁻** and doubly reduced **Cu⁺-AnQ²⁻** species. These anthraquinone reduction potentials are positively shifted by around 400 mV compared to the free anthraquinone

compound in acetonitrile (Fig. S17†) and around 300 mV with respect to the complex featuring an anthraquinone unit linked with Ru(bpy)₃ chromophore(s) reported by Orazietti et al.[22] The slight positive shift of the first two reduction potentials for **Cu⁺-AnQ** is ascribed to the fact that the anthraquinone moiety is fused with the phenazine unit generating a conjugated π-system with a LUMO that occupies lower energy than free anthraquinone or the DPPZ ligand. This is in line with the UV-vis results where the LC band of **Cu⁺-AnQ** occurs at a more red, lower energy wavelength than that of **Cu⁺-DPPZ**.

The reduction of the phenazine unit in **Cu⁺-AnQ** is shown at $E_{1/2}$ = −1.55 V vs. SCE, which exhibits 400 mV negative shift as compared to the phenazine reduction of **Cu⁺-DPPZ** (−1.13 V vs. SCE). The difference in the phenazine reduction potentials between the two complexes is attributed to the negative charges residing on the anthraquinone moiety of **Cu⁺-AnQ²⁻** which makes it more difficult to further reduce the AnQ ligand. Interestingly, both complexes show similar reduction potentials for the blocking ligand mesPhen (−1.77 V vs. SCE for **Cu⁺-AnQ** and −1.70 V vs. SCE for **Cu⁺-DPPZ**), indicating that in such Cu(ɪ) diimine complexes the reduction of one ligand has minimal impact on the electrochemical behavior of the other ligand. It is important to note that the first three reductions of **Cu⁺-AnQ** all occur on the AnQ ligand, demonstrating the capacity of the AnQ ligand to store up to three electrons upon reduction. The moderate reduction potentials for the anthraquinone moiety in AnQ ligand opens up a pathway for (electro)chemical and photochemical charge accumulation on the AnQ ligand.

Spectroelectrochemical study of the reduced Cu anthraquinone complex

To further study the charge accumulation of **Cu⁺-AnQ** and obtain the optical signatures of the reduced species, we performed spectroelectrochemical (SEC) studies with **Cu⁺-AnQ** and **Cu⁺-DPPZ**. The singly reduced species **Cu⁺-AnQ⁻** was generated by poising the potential at −0.80 V vs. SCE, about 270 mV beyond the reduction potential of the anthraquinone moiety (see Fig. 2B). Subtracting the absorption spectrum of **Cu⁺-AnQ** from that of **Cu⁺-AnQ⁻**, a difference absorption spectrum (Fig. 3A, orange curve) corresponding to the singly reduced species **Cu⁺-AnQ⁻** is obtained. The spectrum reveals a depletion of the ligand-based band at 380 nm, indicating that the reduction takes place at the AnQ ligand. Surprisingly, a very wide 'V-shaped' absorption feature across a broad spectral range from visible to near IR region is observed with the lowest absorption at around 630 nm and a steady growth of absorption above 630 nm. Some distinctive features are captured, which include peaks at 430 nm, 486 nm, 1008 nm and a shoulder at 888 nm. These absorptions are derived from the low energy ligand-based transitions of the reduced AnQ ligand. In addition, the increase of the 400 to 550 region indicates that the copper-based MLCT transition is preserved in the singly reduced species and can be used for pumping a second electron to the anthraquinone center, enabling photochemical charge accumulation.

The doubly reduced species **Cu⁺-AnQ²⁻** is afforded after stepping the potential to −1.40 V. As shown by the green trace in Fig. 3A, **Cu⁺-AnQ²⁻** exhibits two equally-intense, relatively narrow peaks centered at 804 nm and 871 nm, a small shoulder at 727 nm, and a broad peak with weak intensity at 452 nm. These features are attributed to the electronic transition taking place on the doubly reduced AnQ ligand of **Cu⁺-AnQ²⁻**. Interestingly, a slightly different bleach feature with respect to that of **Cu⁺-AnQ⁻** is observed. The dip of the depletion of **Cu⁺-AnQ²⁻** appears at 399 nm, which is red-shifted by about 20 nm from that of **Cu⁺-AnQ⁻**. The shift of the bleach band is a response to the difference of the electronic structure between the singly reduced and doubly reduced species and this feature can be used as an additional marker to distinguish the state of reduction of the complex.

Upon further reduction, the difference spectrum at −1.75 V displays a new peak at 571 nm while other absorption features assigned to the doubly reduced species diminish (Fig. 3A magenta curve). This newly detected absorption band arises from the triply reduced complex **Cu⁺-AnQ³⁻**, where the phenazine moiety is the main position that accepts the third electron, forming an AnQ³⁻ ligand. We can make this assignment and confirm the reduction of the phenazine unit by comparison to the SEC response of **Cu⁺-DPPZ** held at −1.40 V. As shown in Fig. 3B, the singly reduced **Cu⁺-DPPZ¹⁻** shows an intense absorption at 568 nm with a spectral shape similar to that of **Cu⁺-AnQ³⁻**. Comparing the results of **Cu⁺-DPPZ¹⁻** with the third reduction of **Cu⁺-AnQ** confirms that the first two reduction events are localized on the anthraquinone and the third occurs at the phenazine unit.
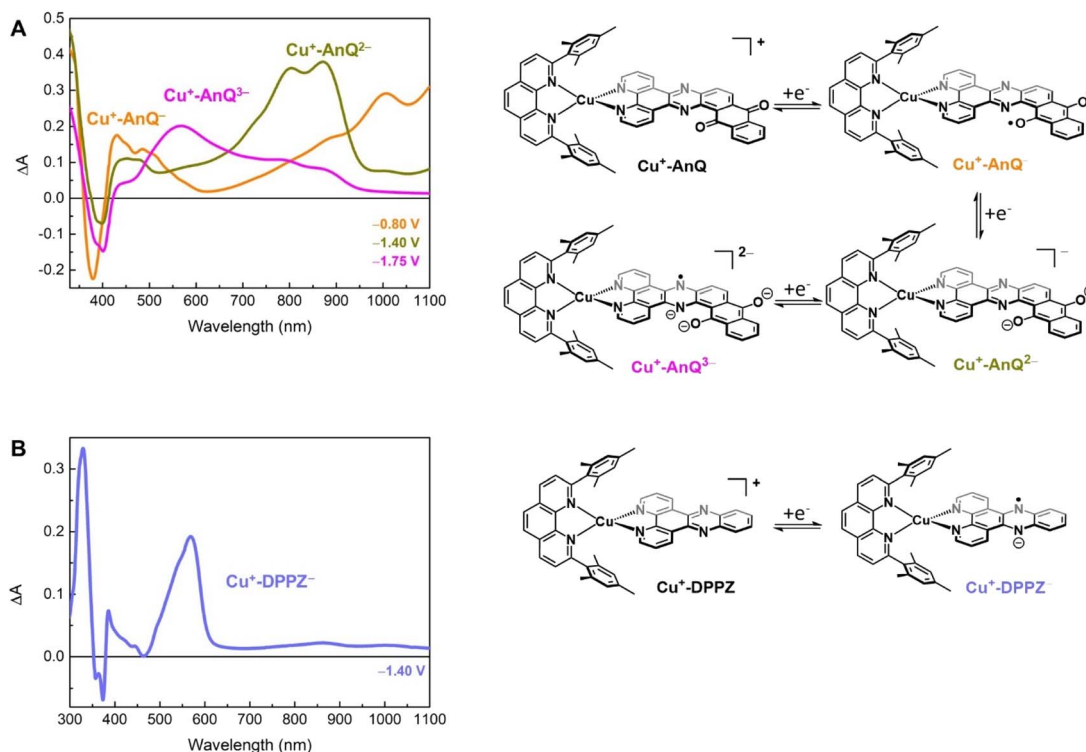

Fig. 3 SEC study of (A) **Cu⁺-AnQ** and (B) **Cu⁺-DPPZ** in 0.1 M TBAPF₆/anhydrous acetonitrile (working: Pt mesh; counter: Pt wire; reference: Ag⁺/Ag pseudoreference electrode). The potential steps shown in the figure are referenced to SCE.
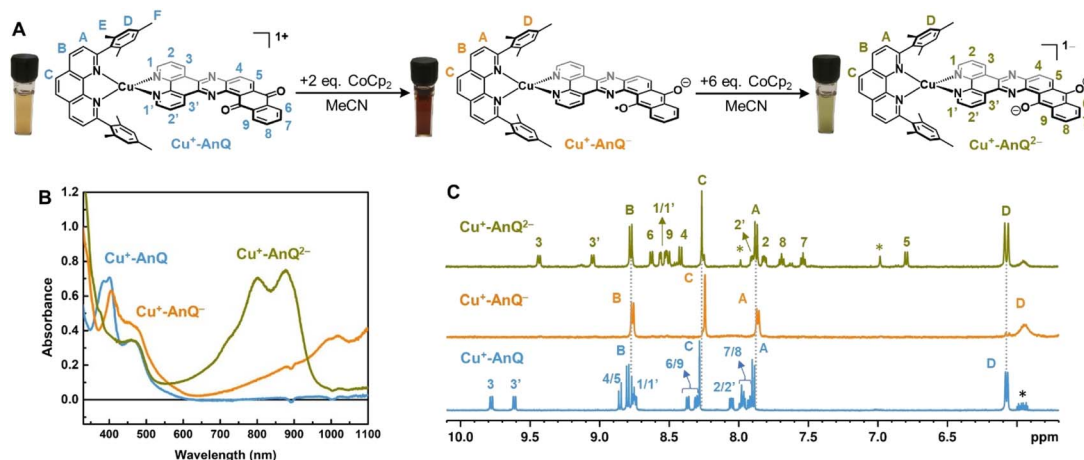
Fig. 4 (A) Reduction of **Cu⁺-AnQ**. (B) UV-vis spectra of **Cu⁺-AnQ** treated with CoCp₂ in CH₃CN. (C) ¹H NMR of the reduced species generated by CoCp₂. (Solvent: CD₃CN; impurity is denoted by asterisk).

Chemical reduction of Cu⁺-AnQ

The reduced species **Cu⁺-AnQ⁻** and **Cu⁺-AnQ²⁻** can also be afforded by chemical reduction. We observed that an acetonitrile solution of **Cu⁺-AnQ** changed color from orange to dark orange and, finally green on titration with cobaltocene (CoCp₂) at room temperature under the protection of N₂ (Fig. 4). The UV-vis spectra of the titration show that complete conversion of **Cu⁺-AnQ** to **Cu⁺-AnQ⁻** was achieved by about two equivalents of CoCp₂ and conversion to **Cu⁺-AnQ²⁻** required six equivalents of CoCp₂ (Fig. S22†). While reduction with CoCp₂ is ideally stoichiometric, excess CoCp₂ was required in this case to complete the reaction because of residual oxygen present in our experimental set up. The UV-vis spectra of the chemically generated **Cu⁺-AnQ⁻** and **Cu⁺-AnQ²⁻** are in good agreement with the electrochemically generated species, which are characterized by the increasingly intense absorption from 650 to 1100 nm for **Cu⁺-AnQ⁻** and the two-peak feature from 700 to 1000 nm for **Cu⁺-AnQ²⁻**. We observed that the doubly reduced species is quite stable under inert atmosphere at room temperature, as demonstrated by nearly identical UV-vis spectra between the freshly generated solution and the solution stored under N₂ for two days (Fig. S23†).

To further characterize the structure of the reduced species, ¹H NMR spectroscopy was performed with the reduced species dissolved in CD₃CN. In Fig. 4C, the spectra of **Cu⁺-AnQ⁻** and **Cu⁺-AnQ²⁻** are compared with the as-synthesized complex **Cu⁺-AnQ**. The singly reduced species **Cu⁺-AnQ⁻** displays only the signals of the mesPhen protons in the aromatic region of the spectrum, whereas the resonances of the protons of AnQ are absent since the unpaired electron is localized on the anthraquinone moiety of **Cu⁺-AnQ⁻**.

The peaks of the mesPhen protons (H^A, H^B, H^C) remain almost unchanged in terms of peak width and position compared with those from **Cu⁺-AnQ** due to the lack of electronic coupling between the mesPhen and AnQ ligand. However, the signals corresponding to the aromatic protons (H^D) on the mesityl groups are broadened and shifted upfield to 5.93 ppm

with respect to 6.07 ppm in **Cu⁺-AnQ**, as a result of the mesityl groups stacking with the AnQ ligand through π–π interaction (see Fig. 1 above). Reduction of the AnQ ligand will accordingly implement a stronger influence on the NMR shifts of the mesityl protons (H^D, H^E and H^F) than those of phenanthroline protons of mesPhen. Indeed, the chemical shift of protons $H^{E'}$ and $H^{F'}$ of **Cu⁺-AnQ⁻** are also broadened and shifted upfield ($H^{E'}$ 1.59 ppm and $H^{F'}$ 1.27 ppm) compared with the corresponding protons of **Cu⁺-AnQ** (H^E 1.77 ppm and H^F 1.29 ppm) (Fig. S29†).

The ¹H NMR spectrum of the doubly reduced **Cu⁺-AnQ²⁻** reveals well-resolved peaks assignable to the protons from both ligands, indicating the two unpaired spins are antiferromagnetically coupled (singlet state) resulting in a diamagnetic complex (green trace, Fig. 4B). Due to the anionic character of the AnQ ligand, all the protons on AnQ are shifted upfield in the NMR spectra compared with **Cu⁺-AnQ**, while the chemical shifts of mesPhen protons are relatively unaffected. Looking at the aliphatic region (Fig. S29†), the chemical shift of $H^{F''}$ is moved to 1.45 ppm with respect to H^F of **Cu⁺-AnQ** (1.29 ppm) and $H^{E''}$ is observed at 1.74 ppm, a 0.03 shift from 1.77 ppm of H^E. The UV-vis and NMR spectroscopy following chemical reduction clearly establish the capacity of **Cu⁺-AnQ** to store multiple charges on the ligand while maintaining the structural integrity of the complexes, paving our way into photochemical charge accumulation.

EPR spectroscopy of the reduced species

Additional direct evidence showing that the extra electrons of the singly and doubly reduced species are localized on the anthraquinone unit of the AnQ ligand was obtained by CW X-band (9.7 GHz) EPR spectroscopy. The chemically generated **Cu⁺-AnQ⁻** and **Cu⁺-AnQ²⁻** were prepared in 1 : 1 MeCN : dichloromethane (DCM) mixture to facilitate glass formation at 100 K. The presence of DCM in the solution does not change the speciation of the complex and the UV-vis spectra of the reduced complexes in this solvent mixture is consistent with that obtained in neat MeCN (Fig. S30†).
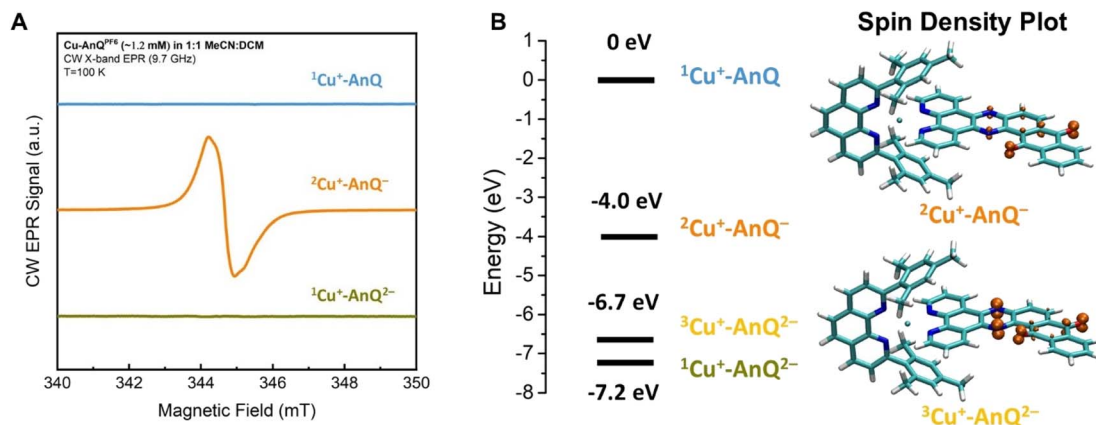
Fig. 5 (A) CW EPR spectra of **Cu⁺-AnQ**, **Cu⁺-AnQ⁻** and **Cu⁺-AnQ²⁻**. (B) Energy level of **Cu⁺-AnQ**, **²Cu⁺-AnQ⁻**, **³Cu⁺-AnQ²⁻** and **¹Cu⁺-AnQ²⁻** and the spin density plot of **²Cu⁺-AnQ⁻** and **³Cu⁺-AnQ²⁻**.

A comparison of the EPR spectra of parent complex **Cu⁺-AnQ**, and reduced complexes **Cu⁺-AnQ⁻** and **Cu⁺-AnQ²⁻** is presented in Fig. 5A. We detected no signs of paramagnetic Cu²⁺, another evidence of the excellent stability of the reduced species. The parent compound **Cu⁺-AnQ** shows no EPR signal, consistent with the diamagnetic character of the Cu(I) complex.

The singly reduced **Cu⁺-AnQ⁻** shows a strong EPR signal centered at $g \approx 2.004$–2.005 (orange spectrum in Fig. 5A), which is in the expected range for an organic anthraquinone radical anion without significant spin density on heavier atoms (like Cu) and is comparable to values reported for similar quinone radical anions (Table S4†).[66–68] The slight deviation from the free electron value of $g_e = 2.002319$ is mostly due to spin density on the oxygen atoms.[69] Indeed, the DFT calculations revealed that the unpaired electron spin in **Cu⁺-AnQ⁻** is delocalized over the anthraquinone moiety and the nitrogen containing bridging phenazine ring (Fig. 5B). This g-tensor anisotropy is too small to be resolved at X-band frequency. Moreover, the DFT calculation of hyperfine interactions showed three strongly coupled magnetic nuclei, the two nitrogen atoms of the bridging ring and one of the hydrogen atoms in the aryl ring between phenazine and quinone (see ESI Table S4†). This is consistent with the observed partially resolved hyperfine structure in Fig. 5A since the most abundant isotopes of carbon (¹²C) and oxygen (¹⁶O) are not magnetic and can be ignored. Based on the DFT calculation, all other nuclei show weaker hyperfine couplings. In particular, the Cu nucleus shows hyperfine couplings of less than 1 MHz, which is expected since the unpaired spin density is largely localized on the anthraquinone moiety of the molecule.

The doubly reduced **Cu⁺-AnQ²⁻** is EPR silent (green spectrum, Fig. 5A). The DFT calculation (Fig. 5B) reveals that the triplet spin state **³Cu⁺-AnQ²⁻** is about 0.5 eV higher in energy than the singlet **¹Cu⁺-AnQ²⁻**, corroborating that the two spins on anthraquinone moiety are antiferromagnetically coupled, resulting in a diamagnetic molecule. Interestingly, the spin density plot of higher energy triplet state **³Cu⁺-AnQ²⁻** presented in Fig. 5B also preserves a major contribution from the oxygen

atoms, but greater spin density is located at the phenazine nitrogen atoms than **Cu⁺-AnQ⁻**.

The experimental EPR data and the DFT calculations nicely align with the other results and discussion above, allowing us to confirm that the first and second reduction of **Cu⁺-AnQ** occur at the anthraquinone unit. As shown in the spin density plot (Fig. 5B), both phenazine and anthraquinone units contribute to the overall spin and a substantial fraction of the spin resides on the oxygen-containing ring of the anthraquinone.

Photochemical charge accumulation with sacrificial electron donor

The capacity of **Cu⁺-AnQ** to accumulate multiple charges *via* electrochemical and chemical methods motivated us to investigate photochemical charge accumulation with this complex using 1,3-dimethyl-2-phenylbenzimidazoline (BIH) as a sacrificial electron donor (SED). BIH, with the first oxidation potential at +0.32 V *vs.* SCE,[70–72] is a two electron one proton donor (Scheme 2) and has been commonly used as a SED in the photoreduction of CO₂ and reduction of organic species.[73] Upon losing one electron, the radical cation BIH˙⁺ is acidic and donates one proton to an acceptor, resulting in the deprotonated BI˙. This radical BI˙ is a potent reductant (E (BI⁺/BI˙) = −1.67 V *vs.* SCE) and will easily give away a second electron forming BI⁺.

In a continuous photolysis experiment, **Cu⁺-AnQ** (0.2 mM) and BIH (0.1 M) were mixed in the dark. Surprisingly, the UV-vis spectrum of the mixture, compared with that of **Cu⁺-AnQ**, shows a depletion at 384 nm and increase of absorption at $\lambda > 650$ nm, indicating the formation of singly reduced **Cu⁺-AnQ⁻** upon addition of BIH in the dark (Fig. 6). In view of thermodynamics,
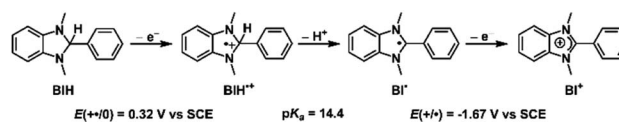
Scheme 2 Oxidation and deprotonation process of BIH.

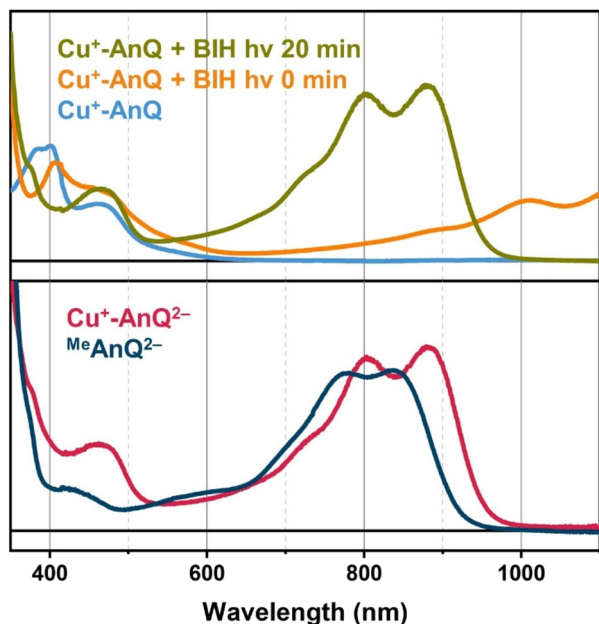Fig. 6 Top: UV-vis spectra of **Cu⁺-AnQ** (blue line), **Cu⁺-AnQ** + BIH with 0 min illumination (orange line), **Cu⁺-AnQ** + BIH with 20 min illumination at 455 nm (green line). Bottom: UV-vis spectra of **Cu⁺-AnQ²⁻** generated from chemical reduction (red line), and **ᴹᵉAnQ²⁻** generated from photoreduction by BIH with 455 nm illumination (dark blue line). For all measurements, the concentrations of the complex, **ᴹᵉAnQ** and BIH in acetonitrile were 0.2 mM, ~0.1 mM and 0.1 M, respectively.

BIH is not a strong enough reductant to donate one electron and generate the singly reduced **Cu⁺-AnQ⁻** in the dark (Fig. S34†). However, the counterintuitive reduction of **Cu⁺-AnQ** by BIH can be rationalized by the extreme excess of BIH compared to the complex (500 : 1) and possibly the formation of a pre-assembly between BIH and **Cu⁺-AnQ** through π–π stacking interactions. Similar phenomena has been observed in previous examples using Ru(II) based photosensitizers.[18,50]

Upon illuminating **Cu⁺-AnQ** and BIH with 455 nm light for 20 min, a double-peaked feature at 804 nm and 880 nm, corresponding to **Cu⁺-AnQ²⁻**, was observed in the spectrum (Fig. 6). The conversion of **Cu⁺-AnQ** to **Cu⁺-AnQ²⁻** is estimated to be quantitative by comparison with the chemical reduction presented in Fig. 4A. The AnQ ligand stays bound with the Cu center after being doubly reduced, which is supported by the persistent Cu(I) MLCT band in this experiment. The intensity of the absorption band of **Cu⁺-AnQ²⁻** in the photolysis experiment showed only small decrease after being stored under room light for 24 h (Fig. S31A†), demonstrating the stability of the doubly reduced complex in the presence of excessive SED. In contrast, the illumination of a **Cu⁺-AnQ** solution without BIH revealed no change in the UV-vis spectrum (Fig. S32†), demonstrating the photostability of **Cu⁺-AnQ** and the role of BIH as an electron source.

The control experiment in the dark was performed with the same solution of **Cu⁺-AnQ** with excess BIH and after 40 minutes a slight increase in the intensity of features at 804 nm, 880 nm

and 1008 nm were observed (Fig. S31A†), which shows that a small amount of **Cu⁺-AnQ⁻** and **Cu⁺-AnQ²⁻** is generated even in the dark. By comparing these spectra to the chemically reduced spectra shown in Fig. 4, the estimated conversion of **Cu⁺-AnQ** to **Cu⁺-AnQ²⁻** in the dark, however, is only about 10% and the concentration of the reduced species are largely unchanged after 24 hours in the dark under N₂ (Fig. S31A†). We propose that the formation of **Cu⁺-AnQ²⁻** without light derives from either the disproportionation of the singly reduced species into doubly reduced species (see the DFT calculation and discussion below), or hydrogen atom transfer from BIH·⁺ species. Therefore, the dark process is also present in the reaction scheme, although it is evident that under illumination **Cu⁺-AnQ** can be fully converted into the doubly reduced complex in a short time, confirming photodriven intra-molecular charge accumulation. Additionally, this photochemical charge accumulation is fully reversible, as demonstrated by exposure of light- and BIH-generated **Cu⁺-AnQ²⁻** to air for 30 minutes (Fig. S31A†). In this experiment, we observed that the spectral features belonging to **Cu⁺-AnQ²⁻** disappeared and only the features assigned to **Cu⁺-AnQ⁻** remain. The complex was not fully converted back to the **Cu⁺-AnQ** ground state, likely because of the large amount of BIH present in solution, but there is no noticeable bleaching in the MLCT band (455 nm), indicating the complex stays intact during oxidation by O₂ and the process of photochemical charge accumulation is reversible.

Next, we examined the possibility of achieving photochemical charge accumulation of **Cu⁺-AnQ** with decreased amount of BIH. In terms of the thermal reduction process of **Cu⁺-AnQ** to **Cu⁺-AnQ⁻** by BIH, we noticed that such process can be depressed by lowering the concentration of BIH. As shown in Fig. S33,† the amount of **Cu⁺-AnQ⁻** generated in the dark process when BIH is at 10 mM is estimated to be about 10% of the total quantity of the complex based on the intensity of the absorption bands. In contrast, there was more than 90% of conversion of **Cu⁺-AnQ** into **Cu⁺-AnQ⁻** in the dark when the concentration of BIH was raised to 0.1 M. Looking at the photolysis step, the rate of charge accumulation declined as the concentration of BIH decreases. The time for the photogenerated doubly reduced species to reach maximum is 18 min, 21 min and 40 min with [BIH] = 50 mM, 10 mM and 5 mM, respectively. Notably, when the concentration of BIH is lowered to 1 mM, only the singly reduced species **Cu⁺-AnQ⁻** was generated. This can be accounted for by the decreased BIH concentration leading to lower driving force for photoreduction so that other reaction pathways, such as photodegradation and comproportionation, outperform the charge accumulation. Overall, we can confirm the photodriven nature of the charge accumulation of **Cu⁺-AnQ** by BIH although we acknowledge that it is complicated by a variety of thermal processes due to the strong reducing power of BIH, coupled proton transfer, and possible pre-assembly between BIH and **Cu⁺-AnQ**.

The important task that remains is to understand the interactions between the Cu(I) center and the ligand of **Cu⁺-AnQ** in the observed photochemical charge accumulation to confirm that the Cu(I) center is indeed functioning as a light absorber in this process. To this end, we subjected the methylated ligand

MeAnQ to similar photolysis experiments as for the **Cu+-AnQ** complex. The methyl groups do not significantly change the electronic properties of **MeAnQ** compared with those of **Cu+-AnQ**, as is evidenced by the comparable electrochemical and optical behaviors to those derived from the ligand in **Cu+-AnQ** (Fig. 2A, S18, S20 and S31†). As in the case of **Cu+-AnQ**, adding BIH to an acetonitrile solution of **MeAnQ** resulted in the formation of singly reduced **MeAnQ⁻**, and illumination of the mixture with 455 nm light led to the doubly reduced species **MeAnQ²⁻** (Fig. S31C†). This indicates that the ligand on its own is also photoactive and functions as a chromophore to absorb light which enables photochemical charge accumulation. As both neutral and singly reduced species of **MeAnQ** exhibit some absorption at around 450 nm in the UV-vis spectra (Fig. 2A, S20†), the ligand can be excited with the 455 nm LED via the red edge of its $\pi \rightarrow \pi^*$ electronic transition. The excited state of the ligand presumably has lower energy than BIH and can be reductively quenched by BIH, generating the doubly reduced anthraquinone moiety (Fig. S34†).

To isolate the contribution of the Cu center in the process of the photochemical charge accumulation, we changed the sacrificial electron donor from BIH to triethylamine (TEA), 0.1 M in solution. TEA has a much higher oxidation potential in acetonitrile than BIH (E(TEA⁺/TEA) $\approx$ +0.8 V vs. SCE vs. E(BIH⁺/BIH) = +0.32 V vs. SCE, see Fig. S19 and S34†). As is shown in Fig. S31D,† no thermal reduction of **MeAnQ** to **MeAnQ⁻** was observed upon mixing the ligand with TEA and the features of **MeAnQ²⁻** were not present during the photolysis of **MeAnQ** with TEA, but instead a new band centered at 525 nm and a depletion at 400 nm were noted. Considering the fact that this new feature is slightly blue-shifted with respect to the feature of the phenazine radical (λ_{max} = 591 nm, Fig. S20†) and an almost complete recovery of the spectrum of the starting material was observed after introducing air into the reaction mixture (Fig. S31D†), the absorption at 525 nm is reminiscent of the protonated phenazine anion where the protons are derived from degradation of TEA[74,75] or trace water after photoinduced electron transfer. Similar species have been observed by the MacDonnell group with a series of phenazine-containing Ru complexes or ligands, and the protonated doubly reduced species exhibit absorption in the range of 500–600 nm, bluer than the singly reduced phenazine radicals.[76,77] Although the thermodynamics of phenazine and anthraquinone in **MeAnQ** dictates that phenazine anion should not be generated, certain photochemical pathway via a ligand-centered transition relevant to the phenazine moiety could presumably be accessed when coupled with protonation. Nonetheless, a detailed investigation of this process is out of the scope of this study. Switching to the photolysis of **Cu+-AnQ** with TEA (Fig. S31D†), generation of **Cu+-AnQ²⁻** was detected, based on the increase of absorption at 800 nm and 880 nm, but complete formation of the doubly reduced complex required longer illumination times with TEA than for BIH (240 vs. 20 minutes). Other features at 550 nm and 730 nm were also captured in the spectrum of the photolysis, suggesting multiple products of this reaction. The absorption at 730 nm is derived from the doubly reduced species interacting with residual water in the reaction mixture through hydrogen-

bonding (the triethylamine was not dried prior to use). The same absorption can be reproduced in the spectroelectrochemical experiment of **Cu+-AnQ** when a small amount of water was added into the solution (Fig. S21†), which exhibited a broad featureless band at 730 nm and a bleaching at 400 nm. The formation of the doubly reduced species using TEA confirms the role of the Cu center as a chromophore that absorbs visible light and transfers its excited electron to the anthraquinone acceptor toward photochemical charge accumulation.

Protonation state of the doubly reduced species generated in the photochemical charge accumulation with BIH

Since BIH is a proton donor in addition to an electron donor (Scheme 3), and quinones are well-known to be good proton acceptors,[13,14] we wanted to specifically investigate the ability of the reduced AnQ ligand to accept the proton from BIH⁺. A mixture of **Cu+-AnQ** and BIH was dissolved in CD₃CN and the resultant mixture was illuminated with 455 nm light for 30 minutes, during which time the reaction was monitored by UV-vis to ensure the complete transformation of the starting material to the doubly reduced species, and NMR spectroscopy was used to identify the final product. Fig. 7 shows that the photoreduced product has comparable NMR signals with that of **Cu+-AnQ²⁻** afforded by the chemical reduction of CoCp₂, with the addition of a well-resolved singlet peak at 14.88 ppm that integrates to exactly one proton. The same NMR features can be reproduced by treating the chemically generated **Cu+-AnQ²⁻** with one equivalent of trifluoroacetic acid (TFA), and the "D₂O shake" experiment demonstrates that the proton is exchangeable with the deuterium of D₂O as it completely disappears after the addition of D₂O. We interpret these results as the newly observed peak arising from a monoprotonated, doubly reduced photoproduct **Cu+-AnQH⁻**. Notably, the 14.88 ppm signal of **Cu+-AnQH⁻** is similar to the δ(OH) (14.9 ppm in CDCl₃) of the structurally-analogous 10-hydroxybenzo[h]quinoline.[78,79] The drastic down field shift of the proton signal indicates that the proton of **Cu+-AnQH⁻** should bond with the O or N atom inside the bay area of the AnQ ligand forming an intramolecular H bonding of –OH···N. Interestingly, the protonation does not shift the other proton resonances from the parent complex, as no apparent change in the peak position of **Cu+-AnQH⁻** is observed with respect to the signals from **Cu+-AnQ²⁻** which suggests a weak electrostatic interaction of the proton with the reduced ligand leading to little distortion of the electron density of the complex.

The structure of **Cu+-AnQH⁻** is further revealed by rotating frame Overhauser effect spectroscopy (ROESY). In our first attempt at this measurement, the acetonitrile-d₃ solution of **Cu+-AnQ** was illuminated using the same conditions for the above experiments, however we observed the crystallization of the photoproduct in the reaction mixture within several hours. The low solubility of the product in acetonitrile prevented us from performing a prolonged NMR measurement. Therefore, we changed the solvent to DMSO-d₆ which solubilized the photoreduced product throughout the measurement. The UV-
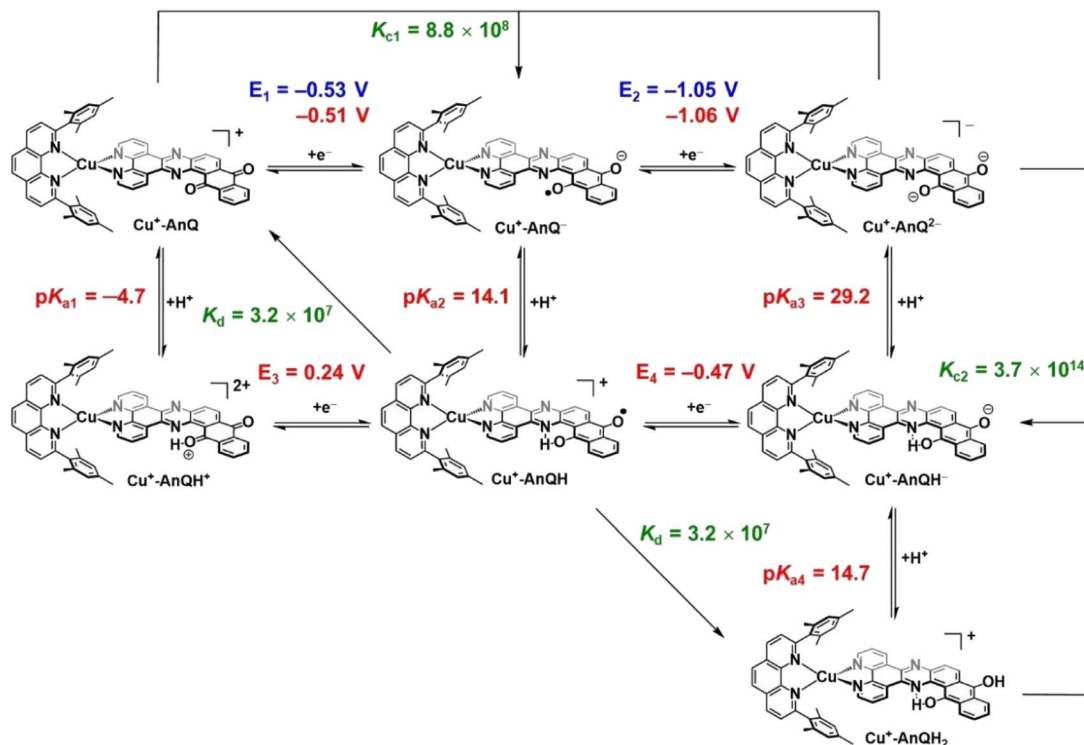
Scheme 3 Square diagram of possible protonation and reduction events starting from **Cu⁺-AnQ**. Experimental E values in blue; calculated E and pK_a in red; calculated comproportionation or disproportionation values in green.
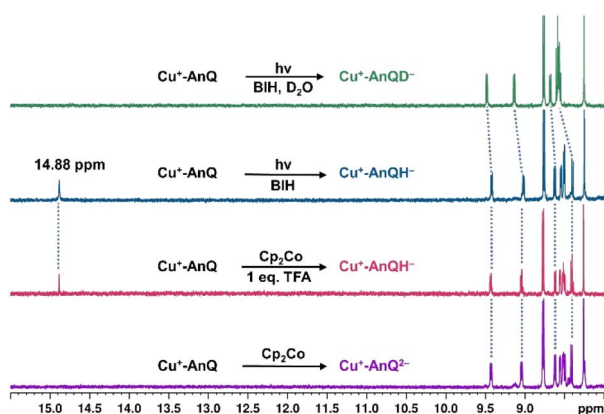

Fig. 7 Comparison of the ^{1}H NMR spectra of **Cu⁺-AnQ²⁻** (purple line), **Cu⁺-AnQH⁻** generated by Cp₂Co and 1 eq. trifluoroacetic acid (red line), **Cu⁺-AnQH⁻** generated by 30 minutes illumination with BIH (teal line), **Cu⁺-AnQD⁻** generated by BIH with 30 min illumination and then added with one drop of D₂O (green line). Illumination with 455 nm light; concentrations of the complex and BIH were kept at 0.2 mM and 0.1 M, respectively, in CD₃CN.

vis and NMR spectra (Fig. S39–S42†) unambiguously demonstrated that the complex undergoes the same photoreduction in DMSO as in acetonitrile, which generates the doubly reduced monoprotonated **Cu⁺-AnQH⁻**. The 2D and 1D ROESY spectra of the resultant mixture in DMSO-d_6 reveals that the proton that appears at 14.9 ppm is correlated with the H³ proton, the one close to the bay of the ligand (Fig. 8A and C). Apart from that, no

additional coupling of the 14.9 ppm proton with other nuclei was observed. This confirms that the O or N atom in the bay of the ligand accepts the proton during photoreduction and, importantly, intramolecular hydrogen bonding exists between the proton and an acceptor atom leading to a stabilized six-membered ring within the bay.

Single crystal X-ray diffraction was used to determine the solid-state structure of the dark crystals obtained from the acetonitrile-d_3 solution of the photoreduced species. As is shown in Fig. 8B, the crystal structure clearly shows a tautomerization between the enol form (H¹⁴) and keto form (H⁵) of **Cu⁺-AnQH⁻**, with an approximate 2 : 3 ratio of the enol and similar energy levels in the energy surface and both the protonation states are produced in the ground state structure. Indeed, DFT calculations (Fig. S44†) were used to investigate the energy of the four possible monoprotonated species (H on N5, N6, O1 or O2), and reveals that **Cu⁺-AnQH⁻$_{O1}$** shows the lowest energy although the ΔG between **Cu⁺-AnQH⁻$_{O1}$** and **Cu⁺-AnQH⁻$_{N5}$** is only 1.5 kcal mol⁻¹. A previous study shows that the installation of electron withdrawing groups on specific positions of HBQ can modulate the relative energy level of the enol and keto isomers.[80] By the same token, the similar energetics of the two isomers of **Cu⁺-AnQH⁻** can be attributed to the extended π-conjugation of AnQ which reduces the electron density of the reduced ligand by distributing the extra charge over the π system (see EPR section). Another key observation from the crystal structure is the difference of C–O bond distances in the AnQ ligand. Since only one proton is associated with the anthraquinone unit of the AnQ ligand, the two C–O bonds show
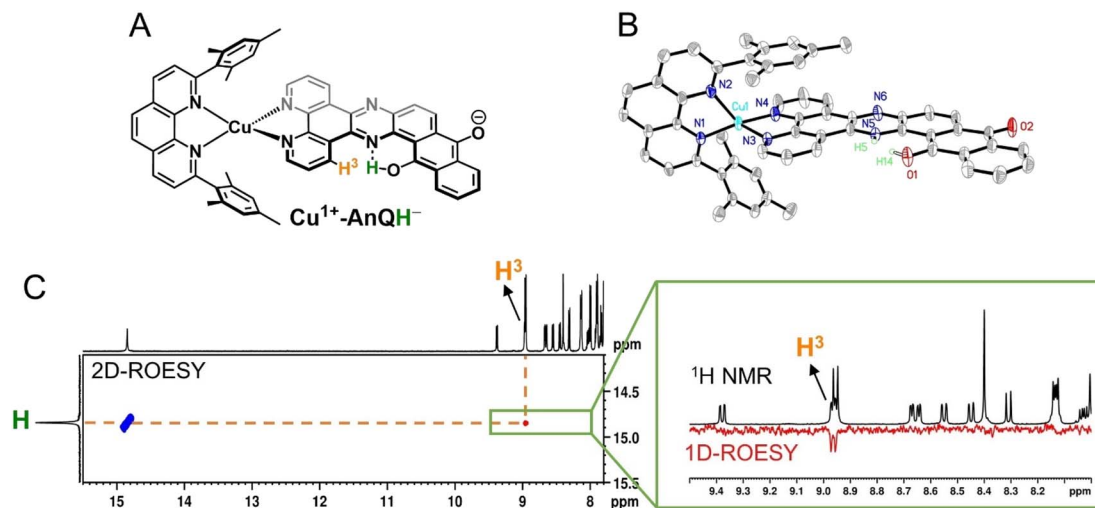
Fig. 8 (A) Molecular structure of the enol form of the monoprotonated $\mathbf{Cu^+}$-$\mathbf{AnQH^-}$. (B) ORTEP diagram of $\mathbf{Cu^+}$-$\mathbf{AnQH^-}$ (50% thermal ellipsoids; all the hydrogen atoms except for H[5] and H[14] are omitted for clarity). Tautomerization of the proton, affording the keto and enol forms, is exhibited as substitution disorder in the crystal structure where the proton of the keto form is labeled as H[5] and the proton of the enol form is labeled as H[14]. The relative ratio of the keto and enol tautomer is 3 : 2. (C) ROESY spectrum of photogenerated $\mathbf{Cu^+}$-$\mathbf{AnQH^-}$ in DMSO-d_6 showing the correlation of the exchangeable proton (14.9 ppm) with other protons in the parent complex. Inset: comparison of the ^{1}H NMR and 1D ROESY spectra from 8.0 ppm to 9.5 ppm. Complex $\mathbf{Cu^+}$-$\mathbf{AnQH^-}$ was produced by illuminating a DMSO-d_6 solution of 0.5 mM $\mathbf{Cu^+}$-$\mathbf{AnQ}$ and 0.1 M BIH with 455 nm light for 4 hours.

very different lengths in the crystal structure. The distance of C–O1 is 1.300(3) Å which is slightly shorter than the normal range of C–O bond lengths for hydroquinones ($\sim$1.35 Å)[81,82] but much longer than the C=O groups in quinones ($\sim$1.23 Å).[21] However, the C–O2 bond is much shorter (1.255(3) Å) than C–O1 due to its deprotonation and falls in the range of carbonyl groups found in quinones.[21] Based on the bond distances, the nature of bonding of C–O1 should be single bond and C–O2 be double bond.

DFT calculated pK_a and E of the Cu-AnQ intermediates

Photoinitiated charge accumulation by $\mathbf{Cu^+}$-$\mathbf{AnQ}$ presumably occurs *via* several proton and electron transfer steps, and we therefore employed DFT calculations to quantify the pK_a and reduction potential E values of the protonated intermediates. Full calculation details are presented in the ESI,† and Scheme 3 summarizes the experimental and calculated reduction and protonation processes following photoexcitation of $\mathbf{Cu^+}$-$\mathbf{AnQ}$. The calculated reduction potentials of the unprotonated redox couples, $\mathbf{Cu^+}$-$\mathbf{AnQ^{0/1-}}$ and $\mathbf{Cu}$-$\mathbf{AnQ^{-/2-}}$, are in good agreement with the experimental values, differing by only 10–20 mV. The large difference in the reduction potentials of the two redox couples results in comproportionation of $\mathbf{Cu^+}$-$\mathbf{AnQ}$ and $\mathbf{Cu^+}$-$\mathbf{AnQ^{2-}}$, generating $\mathbf{Cu^+}$-$\mathbf{AnQ^-}$; the equilibrium constant K_{c1} for the comproportionation is calculated as 8.8×10^8.[83]

The vertical direction of Scheme 3 shows protonation of the Cu complexes. In general, as reduction occurs from $\mathbf{Cu^+}$-$\mathbf{AnQ}$, we observe an increase in the pK_a values, demonstrating an increase of basicity as the complex is reduced. Specifically, the pK_a values of the as-synthesized complex $\mathbf{Cu^+}$-$\mathbf{AnQ}$, the singly reduced $\mathbf{Cu^+}$-$\mathbf{AnQ^-}$ and the doubly reduced $\mathbf{Cu^+}$-$\mathbf{AnQ^{2-}}$ are -4.7, 14.1 and 29.2, respectively. Comparing with the pK_a of radical

BIH$^{\bullet+}$ (14.4 (ref. 70–72)), $\mathbf{Cu^+}$-$\mathbf{AnQ}$ is highly unlikely to be protonated under the conditions in which the photoreduction experiment was conducted. The proton transfer from BIH$^{\bullet+}$ to $\mathbf{Cu^+}$-$\mathbf{AnQ^-}$ should have lower thermodynamic barrier, but due to the similar pK_a values, this process is still uphill which results in slow proton transfer and generating only small amount of $\mathbf{Cu^+}$-$\mathbf{AnQH}$. The doubly reduced species should be easily protonated by BIH$^{\bullet+}$, producing $\mathbf{Cu^+}$-$\mathbf{AnQH^-}$.

The DFT calculations show that the reduction potentials of the protonated complexes are shifted positively compared to their unprotonated analogs. Specifically, the E ($\mathbf{Cu^+}$-$\mathbf{AnQH^+}$/$\mathbf{Cu^+}$-$\mathbf{AnQH}$) and E ($\mathbf{Cu^+}$-$\mathbf{AnQH}$/$\mathbf{Cu^+}$-$\mathbf{AnQH^-}$) are calculated as 0.24 V and -0.47 V vs. SCE, respectively, which are positively shifted by $\sim$600 mV with respect to the corresponding reductions of the deprotonated species. The positive change of the potential can be explained by the stabilization effect of the associated proton on the reduced complexes. The calculations also show that the reduction of the singly reduced, monoprotonated complex $\mathbf{Cu^+}$-$\mathbf{AnQH}$ occurs at a more positive potential than the reduction of the starting complex: $\mathbf{Cu^+}$-$\mathbf{AnQ}$ (E ($\mathbf{Cu^+}$-$\mathbf{AnQH}$/$\mathbf{Cu^+}$-$\mathbf{AnQH^-}$) = -0.47 V and E ($\mathbf{Cu^+}$-$\mathbf{AnQ}$/$\mathbf{Cu^+}$-$\mathbf{AnQ^-}$) = -0.51 V). This potential inversion has been previously observed by other studies with Ru complexes[21,84,85] and has been regarded as an important strategy to achieve photoinduced charge accumulation at mild potentials in photoactive supramolecular assemblies.[7]

Further protonation of $\mathbf{Cu^+}$-$\mathbf{AnQH^-}$ to form $\mathbf{Cu^+}$-$\mathbf{AnQH_2}$ is possible at a moderate pK_{a4} (14.7) for $\mathbf{Cu^+}$-$\mathbf{AnQH_2}$. This suggests that $\mathbf{Cu^+}$-$\mathbf{AnQH^-}$ is less basic than $\mathbf{Cu^+}$-$\mathbf{AnQ^{2-}}$. However, under reaction conditions limited by BIH$^{\bullet+}$ concentration, as in the case of the photolysis experiment, any $\mathbf{Cu^+}$-$\mathbf{AnQH_2}$ that is generated has a propensity to react with $\mathbf{Cu^+}$-$\mathbf{AnQ^{2-}}$ in a comproportionation reaction to yield $\mathbf{Cu^+}$-$\mathbf{AnQH^-}$. The extremely

high driving force for the comproportionation reaction (K_{c2} = 3.7×10^{14}) is a reasonable explanation for the observation of **Cu⁺-AnQH⁻** as the major product in photochemical charge accumulation experiment.

The thermodynamic data provide insights into the process which generates the doubly reduced monoprotonated species in the dark. This is related to the disproportionation of the monoprotonated singly reduced **Cu⁺-AnQH** into **Cu⁺-AnQ** and **Cu⁺-AnQH₂**. With the pK_a and reduction potential E, the equilibrium constant of the disproportionation of **Cu⁺-AnQH** is estimated to be 3.2×10^7. The moderate K_d indicates that **Cu⁺-AnQH**, derived from the protonation of **Cu⁺-AnQ⁻** by BIH·⁺, is highly inclined to undergo disproportionation and affords **Cu⁺-AnQ** and **Cu⁺-AnQH₂**. The subsequent reaction involves proton transfer from **Cu⁺-AnQH₂** to **Cu⁺-AnQ²⁻**, producing **Cu⁺-AnQH**. Although the disproportionation of the protonated Cu species does not require light, the major pathway for charge accumulation should be photochemical. This is based on the fact that the complete conversion of **Cu⁺-AnQ** to **Cu⁺-AnQH⁻** is only realized under illumination (*vide supra*). Overall, the calculated pK_a and E agree well with what we observed in the experimental results which shows the **Cu⁺-AnQH⁻** is the final product.

Discussion

Reaction pathway of the photochemical charge accumulation

Based on the experimental and computational results, we are now equipped to propose a mechanism of the photochemical charge accumulation of **Cu⁺-AnQ** using BIH as a sacrificial electron donor, summarized in Scheme 4. First, the reduction of **Cu⁺-AnQ** to **Cu⁺-AnQ⁻** undergoes *via* thermal-driven mechanism or photodriven mechanism depending on the concentration of BIH in the reaction mixture. Since we observe quite efficient formation of **Cu⁺-AnQ⁻** upon introduction of a large excess of BIH, even prior to illumination, we attribute it to preassembly of BIH with the complex resulting in thermal-induced electron transfer generating **Cu⁺-AnQ⁻**. However, as [BIH] decreases, we observe less reduction in the dark and more **Cu⁺-AnQ⁻** is afforded by photodriven process due to the lower propensity of pre-assembly formation under these conditions.

The following steps involve two diverging pathways, either the photoinduced pathway or thermal-induced pathway. The photoinduced pathway is comprised of the photoexcitation of Cu center, intramolecular electron transfer (ET) from Cu*⁺ to **AnQ⁻**, intermolecular electron transfer from BIH to Cu²⁺ and protonation (PT) of **AnQ²⁻** by BIH·⁺. We hypothesize this pathway as the major contributing factor to drive charge accumulation reaction to completion. As shown in Fig. 6 and S31,† excitation with 455 nm light accelerates the formation of **Cu⁺-AnQ²⁻**, resulting in a quantitative generation of the doubly reduced species. However, this species is only afforded at very low yield in the dark (Fig. S31†). Although excitation of the copper-based MLCT initiates intramolecular photoinduced electron transfer from the Cu(ı) excited state to the **AnQ⁻** ligand which generates **Cu²⁺-AnQ²⁻**, we do not observe this intermediate, likely because the Cu²⁺ center is a very good electron acceptor for BIH (or BIH·⁺) which rapidly forms **Cu⁺-AnQ²⁻**.

This intermediate is highly basic (pK_{a3} 29.2) and readily accepts an electron from BIH·⁺ that is generated from previous electron transfer steps and finally yields **Cu⁺-AnQH⁻**.

The thermal-induced pathway includes three possible mechanisms: PT-D-PT, PT-ET, and HAT process (Scheme 4), and we propose that these three pathways are all kinetically slower than the photoinduced pathway. The first two thermal pathways start with a common intermolecular proton transfer (PT) from BIH·⁺ to **AnQ⁻**. The subsequent steps bifurcate into either electron transfer (ET) from radical BI· to **Cu⁺-AnQH**, or disproportionation (D) of **Cu⁺-AnQH** into **Cu⁺-AnQ** and **Cu⁺-AnQH₂**, and proton transfer (PT) from **Cu⁺-AnQH₂** to **Cu⁺-AnQ²⁻**. The rate of these two pathways can be greatly limited by the first PT step owing to the slightly uphill thermodynamics. Considering the pK_a of the two individual species, the small ΔpK_a between BIH·⁺ and **Cu⁺-AnQH⁻** suggests that the proton transfer to **Cu⁺-AnQ⁻** has a small thermodynamic driving force. It has been reported that the rate of deprotonation of BIH·⁺ is linearly dependent on the pK_a of the conjugate acid of the proton acceptor, and with a small ΔpK_a (<2 units) the proton transfer from BIH·⁺ to proton acceptor shows a rate constant of 10^3 M⁻¹ s⁻¹.[70] On the other hand, the (photoinduced) electron transfer from BIH to **Cu⁺-AnQ⁻** is estimated to be kinetically efficient based on reported rate constants for photoinduced electron transfer from BIH to similar Cu(ı) diimine complexes, on the order of 10^9 M⁻¹ s⁻¹.[86–88] Further support for a fast electron transfer step comes from a closely related example in a molecular copper purpurin chromophore with an anthraquinone moiety that undergoes photoinduced electron transfer with BIH with a quenching rate constant of 9.23×10^9 M⁻¹ s⁻¹.[86] Therefore, these studies suggest that the photodriven reduction of **Cu⁺-AnQ⁻** by BIH should outcompete the proton transfer of BIH·⁺ to **Cu⁺-AnQ⁻**.

The third possible thermal pathway could proceed through a hydrogen atom transfer (HAT) mechanism which directly transfers a H· from BIH·⁺ to **Cu⁺-AnQ⁻**, forming **Cu⁺-AnQH⁻**. Such mechanism has been observed in photochemical CO₂ reduction involving proton-donating organic sacrificial electron donors[89,90] and photoreduction of phenanthrenequinone by alcohols.[91] Considering the pK_a and E of the Cu species and BIH·⁺, the ΔG for the HAT pathway is estimated to be −1.50 eV (Scheme S4†), indicating a viable pathway for the thermal-induced charge accumulation. However, compared with the photoinduced ET-PT process, we deduce that such HAT process could also be kinetically inefficient as indicated by the literature precedents.[92,93] Accordingly, the slower kinetics of the thermal-induced pathways than the photoinduced pathway implies that a sequential electron transfer then proton transfer process consisting of the photoinduced reduction of **Cu⁺-AnQ⁻** and the ensuing formation of **Cu⁺-AnQH⁻** is the most viable mechanism for the accumulation of the second charge.

Solar energy storage by the Cu anthraquinone system

An important outcome of understanding how molecular systems can be designed for photochemical charge accumulation is to be able to utilize the system to collect multiple redox
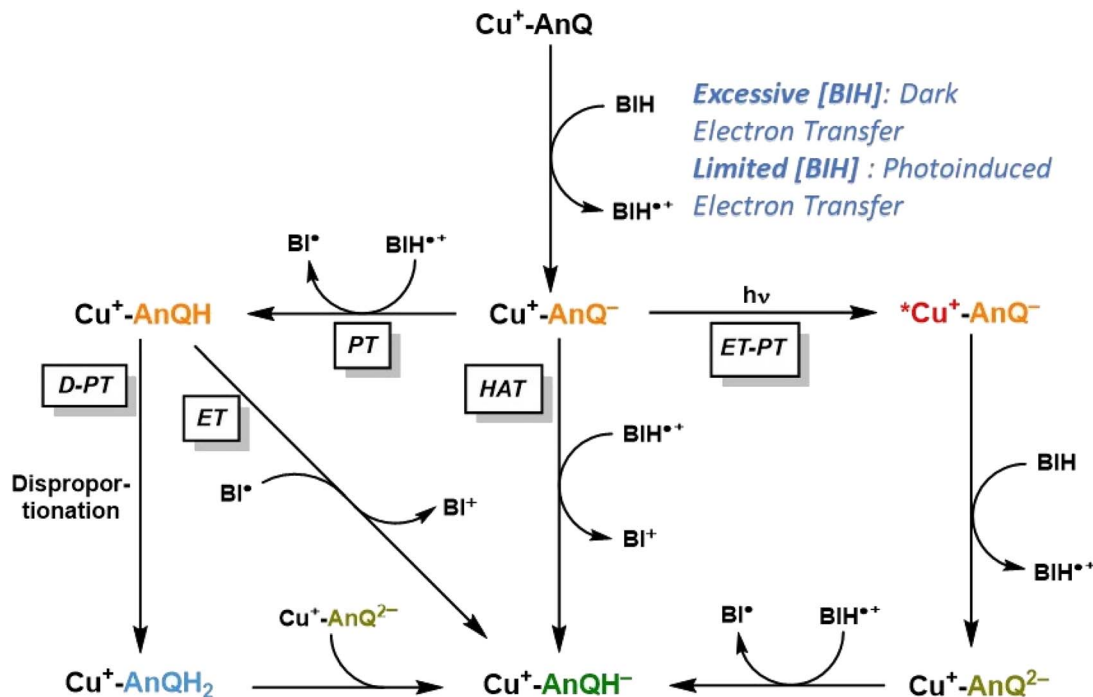
Scheme 4 Proposed reaction mechanism of charge accumulation of **Cu⁺-AnQ** with BIH. PT = proton transfer; ET = electron transfer; D = disproportionation; HAT = hydrogen atom transfer.

equivalents following photoexcitation and perform multi-electron catalysis so that the absorbed energy can be converted into value-added chemicals or fuels. It is, therefore, crucial for the molecular system to not only efficiently accumulate charges but also absorb solar energy with low energy loss. Based on the redox potential and pK_a values obtained in the experiment and calculation, we have calculated the ΔG for the following three processes (Scheme 5, see ESI† for calculation details), *i.e.*, single electron transfer (reaction 1), double electron transfer (reaction 2) and PCET process (reaction 3), in order to assess the capacity of energy storage of **Cu⁺-AnQ** during photochemical charge accumulation. To simplify this discussion, we only consider photodriven reaction, *i.e.*, assuming the first and second reductions only involve photoexcitation.

For reduction-only processes (reactions 1 and 2), the single electron transfer moves one electron from BIH to Cu complex and stores energy of 0.85 eV in **Cu⁺-AnQ⁻**. A second electron transfer increases the total energy accumulated in **Cu⁺-AnQ²⁻** to 2.22 eV. The energy stored in the **Cu-AnQ** system is lower than the previously-reported Ru(II) triarylamine anthraquinone pentad complex, which contains similar anthraquinone group

as the charge accumulation site.[21,22] The Ru pentad system transfers electron from triarylamine to anthraquinone under photochemical conditions and stored substantial amount of energy in the deprotonated doubly reduced species ($\Delta G = 3.56$ eV). We attribute the lower energy storage in our deprotonated species than the Ru pentad complex to the change of the energy level of the electron donors and acceptors. First, the energy of the electron donor (BIH) used with **Cu⁺-AnQ** is higher than that of the Ru pentad (the electron donor in Ru pentad is triarylamine with $E_{ox} = 0.70$ V *vs.* SCE and the BIH $E_{ox} = 0.32$ V *vs.* SCE), making it easier for BIH to donate electrons to the AnQ moiety than triethylamine and thus limits the energy capacity of the system. Second, the extended π-conjugation of the AnQ ligand in **Cu⁺-AnQ** decreases the energy level of the electron acceptor, rendering the reduction potential of the AnQ ligand more positive (E (**AnQ⁰/¹⁻**) = −0.53 V *vs.* SCE, E (**AnQ⁻/²⁻**) = −1.05 V *vs.* SCE) than the reduction potential of anthraquinone in the Ru pentad (E (AQ⁰/¹⁻) = −0.81 V *vs.* SCE, E (AQ¹⁻/²⁻) = −1.31 V *vs.* SCE). This is ascribed to the fact that the anthraquinone in the Ru pentad complex are linked by an aryl group; the connection between the anthraquinone and the Ru chromophore is not a conjugated π-system. This allows the anthraquinone moiety in the Ru pentad to maintain its electronic properties close to a discrete molecule and preserve higher energetics in the system.

Considering the effect of protonation (reaction 3), however, the difference in potential energy stored between the two systems becomes less remarkable. As shown in Scheme 5, protonation of **Cu⁺-AnQ²⁻** dramatically stabilizes the doubly reduced species, reducing the stored energy to 1.35 eV. Whereas
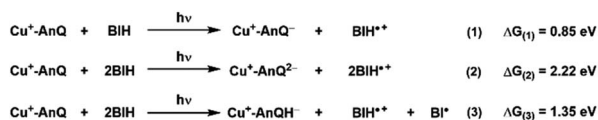
Scheme 5 Reactions and the change of free energy of the photoinduced single ET, double ET and PCET processes between **Cu⁺-AnQ** and BIH.

for the Ru pentad, the energy loss resulting from the protonation is about 2 eV, reducing the total stored energy down to 1.51 eV. The lower energy loss observed here for the **Cu-AnQ** complex can be explained by the fact that the photoproduct of the **Cu-AnQ** system is monoprotonated due to the low basicity of **Cu$^+$-AnQH$^-$** (pK_a = 14.7 for **Cu$^+$-AnQH$_2$**), while the final photoproduct of Ru pentad, according to the authors, is a diprotonated species (AQH$_2$, pK_a was estimated to be 29.3). This demonstrates a unique strategy to preserve the solar energy accumulated in the molecular system by tuning the basicity and structure of the reduced species to control the protonation state of the product.

Conclusions

In summary, we have described the synthesis and complete characterization of the first photoactive earth-abundant Cu(I) diimine complex, **Cu$^+$-AnQ**, that is effective for long-lived and stable photochemical charge accumulation. Electrochemical characterization (CV and SEC) confirms that the AnQ ligand can reversibly accept up to three electrons in the π system of the ligand under electrochemical conditions. The singly reduced **Cu$^+$-AnQ$^-$** and the doubly reduced species **Cu$^+$-AnQ^{2-}** were also generated by chemical reduction and characterized by NMR, EPR and DFT calculations which uncover that the accumulated electrons of the singly and doubly reduced products reside mainly on the anthraquinone moiety. Regeneration of the **Cu$^+$-AnQ** complex upon exposure of the reduced products to air demonstrates the reversibility of the charge accumulation process with the Cu system and opens the door for its study on photochemical charge accumulation. Continuous photolysis of **Cu$^+$-AnQ** in acetonitrile in the presence of BIH as sacrificial electron donor exhibits photodriven reduction of the AnQ ligand by BIH. The structure of the photoproduct is conclusively determined by NMR and X-ray crystallography as the monoprotonated, doubly reduced **Cu$^+$-AnQH$^-$**. Computational investigation of the thermodynamics of the possible intermediates of the **Cu-AnQ** system suggests that an ET process generating **Cu$^+$-AnQ$^-$** and a subsequent ET-PT process is the probable reaction pathway in which the photochemical charge accumulation occurs. The experimental characterization and DFT calculations allow us to estimate that the energy stored in the photochemical charge accumulation by **Cu$^+$-AnQH$^-$** is 1.34 eV.

This work demonstrates that the protonation state and location of a photo- or electrochemically reduced species can be controlled by ligand design and proton stabilization *via* intramolecular hydrogen bonding interactions. Such control of the protonation state can be a potentially universal strategy to preserve harnessed solar energy in a molecular assembly for photochemical charge accumulation. Furthermore, the ability of **Cu$^+$-AnQ** to achieve photochemical charge accumulation is reminiscent of the biological electron transfer molecule plastoquinone (PQ) in photosystem II. Like the photosystem converts the solar energy into reduction equivalents that are utilized for biological CO$_2$ reduction, it is interesting to further investigate reactions that exploit the accumulated charges by the Cu anthraquinone complex to achieve solar energy

conversion. Ongoing work in our group is focused on time-resolved studies to evaluate how ultrafast kinetics of charge separation influences longer-timescale charge accumulation and protonation events. Additionally, given the exciting potential for quinone compounds for direct electrochemical capture of CO$_2$,[94,95] we are pursuing this and related systems in the context of photocatalytic CO$_2$ capture and sequestration.

Data availability

Data are available from the corresponding author upon reasonable request.

Author contributions

Conceptualization—Z.-L. X., K. L. M.; investigation—Z.-L. X., N. G., J. N., O. G. P., V. M. L.; formal analysis—Z.-L. X., J. N., O. G. P., V. M. L.; writing original draft—Z.-L. X., K. L. M.; writing, review and editing—Z.-L. X., N. G., J. N., O. G. P., K. D. G., K. L. M.

Conflicts of interest

There are no conflicts to declare.

Acknowledgements

Notes and references

1 S. Xu and E. A. Carter, *Chem. Rev.*, 2018, **119**, 6631–6669.
2 M. Kondo, H. Tatewaki and S. Masaoka, *Chem. Soc. Rev.*, 2021, **50**, 6790–6831.
3 K. E. Dalle, J. Warnan, J. J. Leung, B. Reuillard, I. S. Karmel and E. Reisner, *Chem. Rev.*, 2019, **119**, 2752–2875.
4 B. Kumar, M. Llorente, J. Froehlich, T. Dang, A. Sathrum and C. P. Kubiak, *Annu. Rev. Phys. Chem.*, 2012, **63**, 541–569.
5 Y. Wang, H. Suzuki, J. Xie, O. Tomita, D. J. Martin, M. Higashi, D. Kong, R. Abe and J. Tang, *Chem. Rev.*, 2018, **118**, 5201–5241.
6 L. Hammarström, *Acc. Chem. Res.*, 2015, **48**, 840–850.
7 T. H. Bürgin and O. S. Wenger, *Energy Fuels*, 2021, **35**, 18848–18856.
8 Y. Pellegrin and F. Odobel, *Coord. Chem. Rev.*, 2011, **255**, 2578–2593.
9 M. R. Wasielewski, *Chem. Rev.*, 2002, **92**, 435–461.
10 J. Barber, *Chem. Soc. Rev.*, 2008, **38**, 185–196.
11 V. Krewald, M. Retegan and D. A. Pantazis, *Top. Curr. Chem.*, 2015, **371**, 23–48.

12 N. Nelson and C. F. Yocum, *Annu. Rev. Plant Biol.*, 2006, **57**, 521–565.

13 P. Heathcote, P. K. Fyfe and M. R. Jones, *Trends Biochem. Sci.*, 2002, **27**, 79–87.

14 M. R. Gunner, J. Madeo and Z. Zhu, *J. Bioenerg. Biomembr.*, 2008, **40**, 509–519.

15 H. Kurreck and M. Huber, *Angew. Chem., Int. Ed.*, 1995, **34**, 849–866.

16 J. Barber and P. D. Tran, *J. R. Soc., Interface*, 2013, **10**, 20120984.

17 M. E. El-Khouly, E. El-Mohsnawy and S. Fukuzumi, *J. Photochem. Photobiol., C*, 2017, **31**, 36–83.

18 R. Konduri, N. R. de Tacconi, A. Krishnan Rajeshwar and F. M. MacDonnell, *J. Am. Chem. Soc.*, 2004, **126**, 11621–11629.

19 R. Konduri, H. Ye, F. M. Macdonnell, S. Serroni, S. Campagna and K. Rajeshwar, *Angew. Chem., Int. Ed.*, 2002, **41**, 3185–3187.

20 N. R. de Tacconi, R. O. Lezna, R. Konduri, F. Ongeri, K. Rajeshwar and F. M. MacDonnell, *Chem.–Eur. J.*, 2005, **11**, 4327–4339.

21 M. Kuss-Petermann, M. Orazietti, M. Neuburger, P. Hamm and O. S. Wenger, *J. Am. Chem. Soc.*, 2017, **139**, 5225–5232.

22 M. Orazietti, M. Kuss-Petermann, P. Hamm and O. S. Wenger, *Angew. Chem., Int. Ed.*, 2016, **55**, 9407–9410.

23 S. Singh, N. R. de Tacconi, N. R. G. Diaz, R. O. Lezna, J. M. Zuñiga, K. Abayan and F. M. MacDonnell, *Inorg. Chem.*, 2011, **50**, 9318–9328.

24 J.-F. F. Lefebvre, J. Schindler, P. Traber, Y. Zhang, S. Kupfer, S. Gräfe, I. Baussanne, M. Demeunynck, J.-M. M. Mouesca, S. Gambarelli, V. Artero, B. Dietzek and M. Chavarot-Kerlidou, *Chem. Sci.*, 2018, **9**, 4152–4159.

25 N. M. Randell, J. Rendon, M. Demeunynck, P. Bayle, S. Gambarelli, V. Artero, J. Mouesca and M. Chavarot-Kerlidou, *Chem.–Eur. J.*, 2019, **25**, 13911–13920.

26 D. Polyansky, D. Cabelli, J. T. Muckerman, E. Fujita, T. Koizumi, T. Fukushima, T. Wada and K. Tanaka, *Angew. Chem., Int. Ed.*, 2007, **46**, 4169–4172.

27 T. Fukushima, T. Wada, H. Ohtsu and K. Tanaka, *Dalton Trans.*, 2010, **39**, 11526–11534.

28 K. Kobayashi, H. Ohtsu, K. Nozaki, S. Kitagawa and K. Tanaka, *Inorg. Chem.*, 2016, **55**, 2076–2084.

29 H. Ohtsu and K. Tanaka, *Angew. Chem., Int. Ed.*, 2012, **51**, 9792–9795.

30 C. E. Housecroft and E. C. Constable, *Chem. Soc. Rev.*, 2015, **44**, 8386–8398.

31 C. Bozal-Ginesta, C. A. Mesa, A. Eisenschmidt, L. Francàs, R. B. Shankar, D. Antón-García, J. Warnan, J. Willkomm, A. Reynal, E. Reisner and J. R. Durrant, *Chem. Sci.*, 2021, **12**, 946–959.

32 M. Schulz, N. Hagmeyer, F. Wehmeyer, G. Lowe, M. Rosenkranz, B. Seidler, A. Popov, C. Streb, J. G. Vos and B. Dietzek, *J. Am. Chem. Soc.*, 2020, **142**, 15722–15728.

33 M. Ruthkosky, C. A. Kelly, F. N. Castellano and G. J. Meyer, *Coord. Chem. Rev.*, 1998, **171**, 309–322.

34 M. Iwamura, S. Takeuchi and T. Tahara, *Acc. Chem. Res.*, 2015, **48**, 782–791.

35 M. W. Mara, K. A. Fransted and L. X. Chen, *Coord. Chem. Rev.*, 2015, **282–283**, 2–18.

36 D. R. McMillin and K. M. McNett, *Chem. Rev.*, 1998, **98**, 1201–1219.

37 C. T. Cunningham, K. L. H. Cunningham, J. F. Michalec and D. R. McMillin, *Inorg. Chem.*, 1999, **38**, 4388–4392.

38 M. Sandroni, Y. Pellegrin and F. Odobel, *C. R. Chim.*, 2016, **19**, 79–93.

39 C. E. McCusker and F. N. Castellano, *Inorg. Chem.*, 2013, **52**, 8114–8120.

40 S. Garakyaraghi, C. E. McCusker, S. Khan, P. Koutnik, A. T. Bui and F. N. Castellano, *Inorg. Chem.*, 2018, **57**, 2296–2307.

41 M. C. Rosko, E. M. Espinoza, S. Arteta, S. Kromer, J. P. Wheeler and F. N. Castellano, *Inorg. Chem.*, 2023, **62**, 3248–3259.

42 M. Ruthkosky, C. A. Kelly, M. C. Zaros and G. J. Meyer, *J. Am. Chem. Soc.*, 1997, **119**, 12004–12005.

43 M. S. Lazorski, R. H. Gest and C. M. Elliott, *J. Am. Chem. Soc.*, 2012, **134**, 17466–17469.

44 A. M. Potocny, B. T. Phelan, E. A. Sprague-Klein, M. W. Mara, D. M. Tiede, L. X. Chen and K. L. Mulfort, *Inorg. Chem.*, 2022, **61**, 19119–19133.

45 X. Zhang, M. Cibian, A. Call, K. Yamauchi and K. Sakai, *ACS Catal.*, 2019, **9**, 11263–11273.

46 H. Yersin, A. F. Rausch, R. Czerwieniec, T. Hofbeck and T. Fischer, *Coord. Chem. Rev.*, 2011, **255**, 2622–2652.

47 M. Schmittel, C. Michel, S.-X. Liu, D. Schildbach and D. Fenske, *Eur. J. Inorg. Chem.*, 2001, **2001**, 1155–1166.

48 M. Schmittel and A. Ganz, *Chem. Commun.*, 1997, 999–1000.

49 S. De, K. Mahata and M. Schmittel, *Chem. Soc. Rev.*, 2010, **39**, 1555–1575.

50 A. G. Bonn and O. S. Wenger, *Phys. Chem. Chem. Phys.*, 2015, **17**, 24001–24010.

51 M. Kuss-Petermann and O. S. Wenger, *Chem.–Eur. J.*, 2017, **23**, 10808–10814.

52 L. Gimeno, C. Queffelec, E. Blart and Y. Pellegrin, *ACS Omega*, 2022, **7**, 13112–13119.

53 R. B. López, B. L. Loeb, T. Boussie and T. J. Meyer, *Tetrahedron Lett.*, 1996, **37**, 5437–5440.

54 L. Yang, D. R. Powell and R. P. Houser, *J. Chem. Soc., Dalton Trans.*, 2007, 955–964.

55 M. G. Fraser, H. Van Der Salm, S. A. Cameron, A. G. Blackman and K. C. Gordon, *Inorg. Chem.*, 2013, **52**, 2980–2992.

56 J. Habermehl, D. Sorsche, P. Murszat and S. Rau, *Eur. J. Inorg. Chem.*, 2016, **2016**, 3423–3428.

57 J. Bolger, A. Gourdon, E. Ishow and J.-P. Launay, *Inorg. Chem.*, 1996, **35**, 2937–2944.

58 S. D. Bergman, D. Reshef, S. Groysman, I. Goldberg and M. Kol, *Chem. Commun.*, 2002, **2**, 2374–2375.

59 D. Gut, A. Rudi, J. Kopilov, I. Goldberg and M. Kol, *J. Am. Chem. Soc.*, 2002, **124**, 5449–5456.

60 R. B. Martin, *Chem. Rev.*, 1996, **96**, 3043–3064.

61 Z. Chen, A. Lohr, C. R. Saha-Möller and F. Würthner, *Chem. Soc. Rev.*, 2009, **38**, 564–584.

62 D. Hayes, L. Kohler, R. G. Hadt, X. Zhang, C. Liu, K. L. Mulfort and L. X. Chen, *Chem. Sci.*, 2018, **9**, 860–875.

63 L. Kohler, R. G. Hadt, D. Hayes, L. X. Chen and K. L. Mulfort, *Dalton Trans.*, 2017, **46**, 13088–13100.

64 L. Kohler, D. Hayes, J. Hong, T. J. Carter, M. L. Shelby, K. A. Fransted, L. X. Chen and K. L. Mulfort, *Dalton Trans.*, 2016, **45**, 9871–9883.

65 Z. L. Xie, X. Liu, A. J. S. Valentine, V. M. Lynch, D. M. Tiede, X. Li and K. L. Mulfort, *Angew. Chem., Int. Ed.*, 2022, **61**, e202111764.

66 Y. Sakuragi, B. Zybailov, G. Shen, D. A. Bryant, J. H. Golbeck, B. A. Diner, I. Karygina, Y. Pushkar and D. Stehlik, *J. Biol. Chem.*, 2005, **280**, 12371–12381.

67 M. Vuolle and R. Mäkelä, *J. Chem. Soc., Faraday Trans. 1*, 1987, **83**, 51–55.

68 Y. N. Pushkar, I. Karyagina, D. Stehlik, S. Brown and A. Van Der Est, *J. Biol. Chem.*, 2005, **280**, 12382–12390.

69 O. Burghaus, M. Plato, M. Rohrer, K. Möbius, F. MacMillan and W. Lubitz, *J. Phys. Chem.*, 1993, **97**, 7639–7647.

70 R. N. Sampaio, D. C. Grills, D. E. Polyansky, D. J. Szalda and E. Fujita, *J. Am. Chem. Soc.*, 2020, **142**, 2413–2428.

71 S. Ilic, A. Alherz, C. B. Musgrave Cde, K. D. Glusac and R. Li, *Chem. Commun.*, 2019, **55**, 5583–5586.

72 X. Q. Zhu, M. T. Zhang, A. Yu, C. H. Wang and J. P. Cheng, *J. Am. Chem. Soc.*, 2008, **130**, 2501–2516.

73 Y. Pellegrin and F. Odobel, *C. R. Chim.*, 2017, **20**, 283–295.

74 P. J. DeLaive, T. K. Foreman, D. G. Whitten and C. Giannotti, *J. Am. Chem. Soc.*, 1980, **102**, 5627–5631.

75 E. D. Cline, S. E. Adamson and S. Bernhard, *Inorg. Chem.*, 2008, **47**, 10378–10388.

76 J. M. Aslan, D. J. Boston and F. M. MacDonnell, *Chem.–Eur. J.*, 2015, **21**, 17314–17323.

77 J. M. Aslan, M. Yousufuddin, D. J. Boston and F. M. MacDonnell, *Inorg. Chim. Acta*, 2017, **454**, 216–221.

78 M. L. Martinez, W. C. Cooper and P. T. Chou, *Chem. Phys. Lett.*, 1992, **193**, 151–154.

79 P. T. Chou, Y. C. Chen, W. S. Yu, Y. H. Chou, C. Y. Wei and Y. M. Cheng, *J. Phys. Chem. A*, 2001, **105**, 1731–1740.

80 S. Hristova, G. Dobrikov, F. S. Kamounah, S. Kawauchi, P. E. Hansen, V. Deneva, D. Nedeltcheva and L. Antonov, *RSC Adv.*, 2015, **5**, 102495–102507.

81 R. D. Adams and S. Miao, *Inorg. Chem.*, 2004, **43**, 8414–8426.

82 J. G. M. De Carvalho, R. A. Fischer and A. Pöthig, *Inorg. Chem.*, 2021, **60**, 4676–4682.

83 A. Babaei, P. A. Connor, A. J. McQuillan and S. Umapathy, *J. Chem. Educ.*, 1997, **74**, 1200–1203.

84 J. Nomrowski, X. Guo and O. S. Wenger, *Chem.–Eur. J.*, 2018, **24**, 14084–14087.

85 J. Nomrowski and O. S. Wenger, *J. Am. Chem. Soc.*, 2018, **140**, 5343–5346.

86 H. Yuan, B. Cheng, J. Lei, L. Jiang and Z. Han, *Nat. Commun.*, 2021, **12**, 1835.

87 H. Takeda, Y. Monma and O. Ishitani, *ACS Catal.*, 2021, **11**, 11973–11984.

88 H. Takeda, H. Kamiyama, K. Okamoto, M. Irimajiri, T. Mizutani, K. Koike, A. Sekine and O. Ishitani, *J. Am. Chem. Soc.*, 2018, **140**, 17241–17254.

89 X. Zheng, M. C. Drummer, H. He, T. M. Rayder, J. Niklas, N. P. Weingartz, I. L. Bolotin, V. Singh, B. V. Kramar, L. X. Chen, J. T. Hupp, O. G. Poluektov, O. K. Farha, P. Zapol and K. D. Glusac, *J. Phys. Chem. Lett.*, 2023, **14**, 4334–4341.

90 W. Xie, J. Xu, U. Md Idros, J. Katsuhira, M. Fuki, M. Hayashi, M. Yamanaka, Y. Kobori and R. Matsubara, *Nat. Chem.*, 2023, **15**, 794–802.

91 J. Talvitie, I. Alanko, A. Lenarda, N. Durandin, N. Tkachenko, M. Nieger, J. Helaja, J. Talvitie, I. Alanko, A. Lenarda, M. Nieger, J. Helaja, N. Durandin and N. Tkachenko, *ChemPhotoChem*, 2023, e202300107.

92 J. M. Mayer, *Acc. Chem. Res.*, 2011, **44**, 36–46.

93 J. J. Warren and J. M. Mayer, *Proc. Natl. Acad. Sci. U. S. A.*, 2010, **107**, 5282–5287.

94 Y. Liu, H. Z. Ye, K. M. Diederichsen, T. Van Voorhis and T. A. Hatton, *Nat. Commun.*, 2020, **11**, 1–11.

95 J. M. Barlow and J. Y. Yang, *J. Am. Chem. Soc.*, 2022, **144**, 14161–14169.